Applied Catalysis B: Environmental 341 (2024) 123328

Contents lists available at ScienceDirect

Applied Catalysis B: Environmental

journal homepage: www.elsevier.com/locate/apcatb

Electrochemical extraction of methanol from lignin under mild conditions

Takashi Hibino [a,*], Kazuyo Kobayashi [a], Dongwen Zhou [a], Siyuan Chen [a], Anatoly Zinchenko [a], Shinya Teranishi [b], Aki Miyawaki [b], Yoshiharu Sawada [c]

[a] Graduate School of Environmental Studies, Nagoya University, Nagoya, Aichi 464-8601, Japan
[b] Soken, Inc., Nisshin, Aichi 470-0111, Japan
[c] Technical Center, Nagoya University, Nagoya, Aichi 464-8601, Japan

ARTICLE INFO

Keywords:
Lignosulfonate
Electro-oxidation
Methanol synthesis
Demethylation
Active oxygen species

ABSTRACT

We report an electrochemical approach to extract methanol from lignin with a maximum efficiency of 95% under mild conditions of ambient pressure and a temperature of 75 °C. Hydroxyl radicals were generated from water over a platinum-sputtered anode and attacked the syringyl and guaiacyl units of the lignin. Methoxy groups in the units were demethylated to methanol with a yield greater than 40% through the formation of hemiketal intermediates. The electro-oxidation was coupled to cathode reactions that generated hydrogen in a helium flow and electric power in an air flow. Another important aspect of this approach is that no extra energy or effort was required to separate methanol from the reaction system. This technology can accelerate the replacement of fossil organic resources with renewable biomass resources.

1. Introduction

Lignin, a class of compounds whose molecular weights range from 100 to 150,000 depending on the biomass species, is the most abundant class of natural aromatic polymers [1]. These materials are generated as waste products of the pulp and paper manufacturing processes [2] and have also recently been isolated from lignocellulose via chemical [3,4], physical [5,6], and biological treatments [7,8]. These products are denoted as technical lignin to distinguish them from native lignin in natural biomass [9]. Among technical lignins, lignosulfonates, which are produced using sulfurous acid or sodium sulfite, have been the most widely used as dispersants, pesticides, surfactants, additives, stabilizers, and plasticizers in different applications [10–12]. However, at present, the synthesis of further value-added products from lignosulfonates and the development of manufacturing processes for such products are more attractive from the perspective of sustainable development strategies [13–15]. For example, vanillin and phenol can be extracted from lignosulfonates via oxidative and reductive depolymerization, respectively [16]; bio-oils, including ketones [17], aldehydes [18], ethers [19], carboxylic acids [20], and alcohols [21], can be generated by pyrolysis or hydrolysis of lignosulfonates; and hydrogen and carbon monoxide can be synthesized by gasification of lignosulfonates [22].

One of the specific functional groups in lignin units is the methoxy group [23]. A lignosulfonate has been reported to contain 8.7 wt% methoxy groups [24], although the weight of Na was not included in the total weight. Lignin derivatives have been demethylated or demethoxylated using strong acids or bases (concentrated H_2SO_4 [24], HBr [25], HI [26], or NaOH [27]), special catalytic or oxidizing reagents ($RuCl_3$ [28] or $NaIO_4$ [29]), or enzymes (*O*-demethylases) [30] to determine the quantity of methoxy groups or to isolate aromatic chemicals. Methanol [24,27,29,30], a methyl halide [25], formaldehyde [30], acetic acid [28], or one of various other compounds [26] was formed along with the aromatic compounds. In addition, some of these reaction systems require harsh conditions (low temperatures: −78 °C [24], high temperatures: 120–280 °C [25–28], or high pressures: 5 MPa [27,28]) and subsequent separation or recovery processes. If methoxy groups are to be extracted from lignosulfonates as useful compounds, improvements are needed in terms of energy consumption and operating costs.

Electrochemical processes have become promising alternatives for the upgradation of lignin [31–36]. To date, lignosulfonates have been electro-oxidized to vanillin and small amounts of vanillic acid [37] and acetovanillone [38]. Compared with thermal catalytic oxidation, the electro-oxidation can be conducted at lower temperatures and lower

* Corresponding author.
E-mail addresses: hibino@urban.env.nagoya-u.ac.jp (T. Hibino), kkoba@urban.env.nagoya-u.ac.jp (K. Kobayashi), zhou.dongwen@j.mbox.nagoya-u.ac.jp (D. Zhou), chen.siyuan@a.mbox.nagoya-u.ac.jp (S. Chen), zinchenko@urban.env.nagoya-u.ac.jp (A. Zinchenko), shinya.teranishi.j5k@soken-labs.co.jp (S. Teranishi), aki.miyawaki.j6b@soken-labs.co.jp (A. Miyawaki), y_sawada@agr.nagoya-u.ac.jp (Y. Sawada).

https://doi.org/10.1016/j.apcatb.2023.123328
Received 19 June 2023; Received in revised form 8 September 2023; Accepted 21 September 2023
Available online 24 September 2023

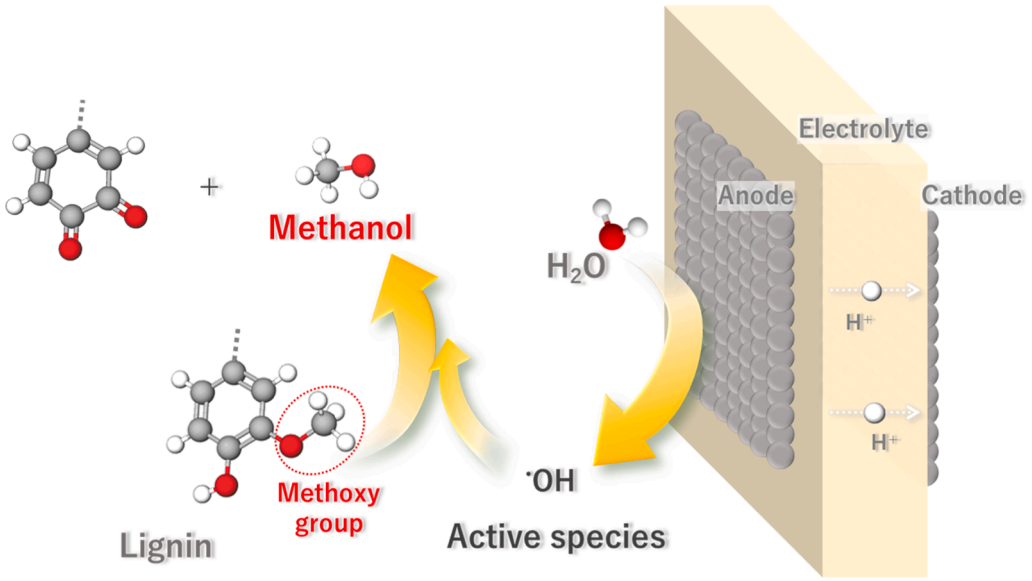

Scheme 1. Schematic of electrochemical extraction of methanol from lignin.

pressures. The oxidants can be generated at the anode in situ, and the electricity can be supplied by renewable energy sources. An additional benefit is the production of hydrogen as a byproduct at the cathode [39–41]. Although some amount of methanol has been extracted from lignin monomer model compounds such as 2-methoxy and 2,6-dimethoxy phenols by cathodic demethoxylation [34], the synthesis of methanol by anodic demethylation of lignin polymers such as lignosulfonate has seldom been reported.

In the present study, we attempted to electrolyze lignosulfonate anodically to form methanol under mild conditions (Scheme 1). To achieve electro-oxidation under such conditions, anode materials were optimized for methanol formation, where the use of carbon supports was avoided because they also possess methoxy groups [42]. Under the optimized conditions, methanol was extracted with high faradaic efficiencies and without complicated separation procedures. Finally, the reaction mechanism for the demethylation of lignosulfonate was elucidated through active species or residue analysis, which demonstrated that hydroxyl radicals (•OH) play an important role as a reaction initiator. Previous lignin electrolysis has focused on the production of aromatic compounds for food and plastic raw materials [31–38]; however, our electrolysis method opens a new avenue for C1 chemistry through the synthesis of methanol and hydrogen.

2. Experimental

2.1. Materials

A lignosulfonate and 85% H_3PO_4 were purchased from Tokyo Chemical Industry and Waco Chemical, respectively. An electrochemical cell consisted of a metal (Ti, Ni, Cu, Mo, W, Pt, or Au, projected area 0.5 cm^2) anode, $Sn_{0.9}In_{0.1}P_2O_7$ (SIPO)–polytetrafluoroethylene (PTFE, DuPont Mitsui) electrolyte, and Pt/C (Electrochem, Pt loading 2 mg cm^{-2}, Vulcan carbon support, projected area 0.5 cm^2) cathode. SIPO powder was synthesized using a previously reported method [43]. Briefly, SnO_2 (Wako Chemical) and In_2O_3 (Wako Chemical) were mixed with H_3PO_4. The mixture was calcined in an alumina pot at 650 °C for 2.5 h and then ground into a powder with a mortar and pestle. The SIPO powder (1.00 g) was then mixed with PTFE powder (0.04 g) and cold-rolled to a thickness of 200 μm using a laboratory rolling mill. Metal meshes (0.1 mm wire diameter, 36.5% porosity) were used for the preliminary assessment of anode materials. In addition, Pt anode particles were deposited onto one side of the electrolyte by sputtering (Sanyu Electron, SC-701MkII) of a Pt target (Nilaco, Pt > 99.9%) under an Ar atmosphere (oxygen < 0.1 ppm). The current was maintained at 5 mA during sputtering, and the sputtering time was fixed at 30 min

2.2. Characterization

The lignosulfonate before electrolysis was characterized as follows. Scanning electron microscopy (SEM) and energy-dispersive X-ray spectroscopy (EDS) observations were conducted using a Jeol JSM-6610A microscope with acceleration voltages of 2 and 15 kV, respectively. ^1H and ^{13}C nuclear magnetic resonance (NMR) spectra were recorded in deuterated dimethyl sulfoxide (DMSO-d_6) using a Bruker AVANCE NEO 500 MHz spectrometer with tetramethylsilane (TMS) as an internal standard. Fourier transform infrared (FT-IR) spectra were obtained using a JASCO FT/IR-460 spectrometer; the spectra were collected in the wavenumber range 4000–500 cm^{-1} with a resolution of 1 cm^{-1}. Simultaneous thermogravimetry (TG) and differential thermal analysis (DTA) were performed using a Shimadzu DTG-60 instrument; the data were collected from room temperature to 400 °C at a heating rate of 10 °C min^{-1} under flowing Ar. In addition to being analyzed by FT-IR and NMR spectroscopies, the lignosulfonate after electrolysis was identified using a gas chromatography (GC; Agilent HP6890) in conjunction with a mass-selective detector (JEOL JMS-700). The microstructure of the Pt deposits was characterized by high-resolution SEM (Thermo Fisher Helios 5 Hydra UX), where the accelerating voltage was 2 kV and the beam current was 0.1 nA. Samples for SEM observation were prepared by focused-ion beam (FIB) milling using a Ga^+-ion beam. X-ray diffraction (XRD) patterns were collected using a Rigaku MiniFlex II diffractometer equipped with a monochromator and a Cu Kα radiation source (1.5432 Å). X-ray photoelectron spectroscopy (XPS) was performed using a VG Scientific ESCALab220i-XL spectrometer equipped with a monochromatic Al Kα radiation source (1486.6 eV). Ultraviolet–visible (UV–vis) absorbance was measured in the wavelength range 400–700 nm using a JASCO V-630 spectrophotometer.

2.3. Electrochemical measurements

The electrolysis cell was set up by sandwiching the cell assembly between two alumina tube systems, where each system was composed of double tubes with outer diameters of 6 and 13 mm (Fig. S1). An Au foil was attached as a reference electrode onto the surface of the electrolyte

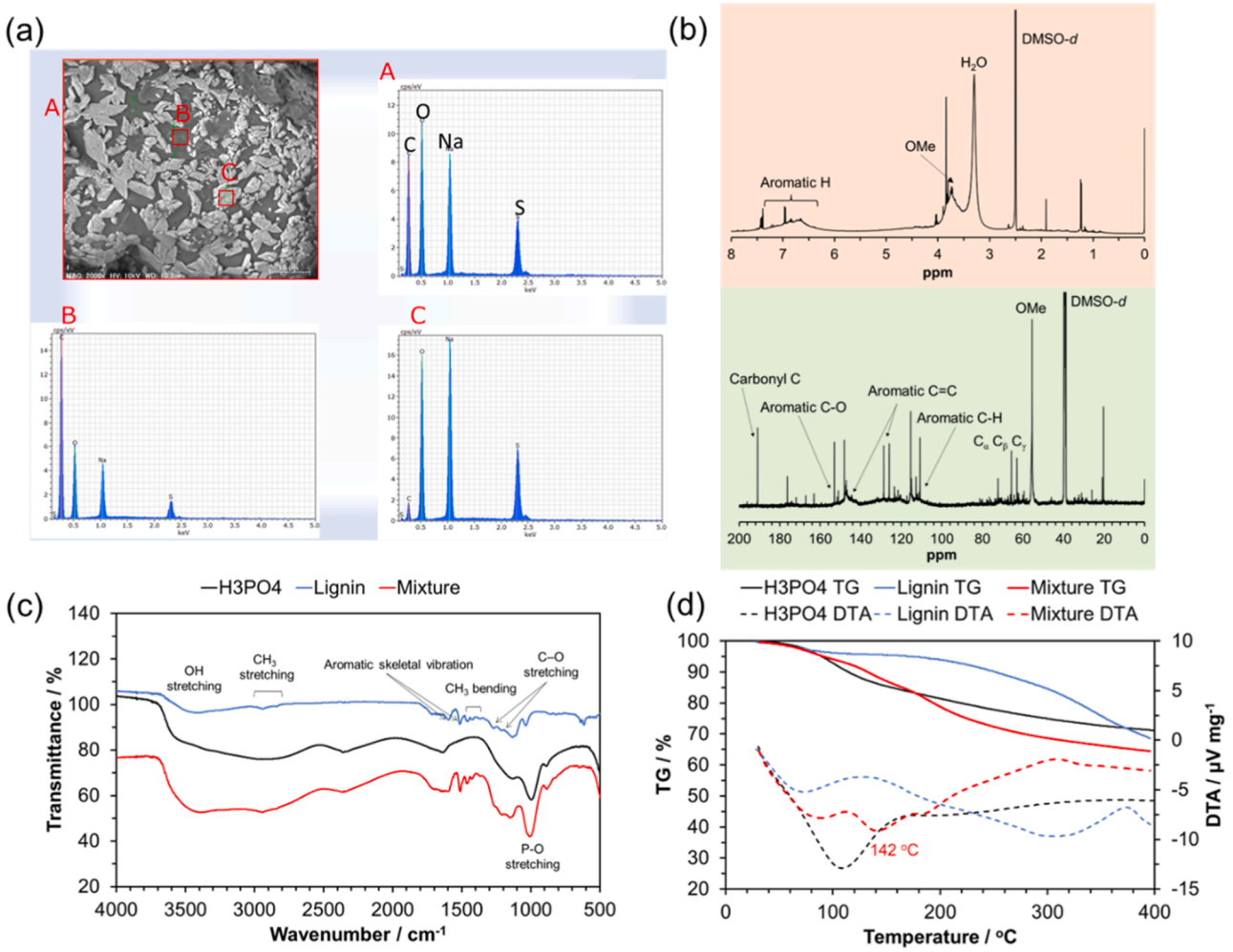

Fig. 1. (a) SEM image and EDX spectra for the lignosulfonate at different locations. (b) ^{1}H and ^{13}C NMR spectra for the lignosulfonate components dissolved in DMSO-d_6. (c) FT-IR spectra and (d) TG–DTA curves for lignosulfonate, 85% H_3PO_4, and their mixture (lignosulfonate:85% H_3PO_4 = 1:3).

in the anode chamber. A mixture of lignosulfonate and 85% H_3PO_4 (weight ratio 1:3) was mounted between the anode and the current collector. Humidified He was fed into the anode at a flow rate of 5 mL min^{-1}, and pure He (oxygen < 0.05 ppm) was fed into the cathode at the same flow rate. The humidification of He was carried out by pre-bubbling He into water at room temperature. The electrolysis cell was heated in the range from 50° to 150°C in an electric furnace cell equipped with a thermocouple. All electrochemical measurements were performed using a potentiostat–galvanostat (Solartron 1287) and a frequency-response analyzer (Solartron 1260). The electrochemical cell was polarized between the anode and reference electrode potentiostatically or potentiodynamically. Impedance spectra were collected at an open-circuit voltage (OCV) over the frequency range 0.1–10^6 Hz with an amplitude voltage of 20 mV. The composition of gaseous products from the electrode was monitored using two online gas chromatographs (a Shimadzu GC-2014 for methanol and dimethyl ether (DME) and a Varian CP-4900 for the other gases); He was used as the carrier gas. The rate and faradaic efficiency of product formation were determined using the following equations:

Product concentration (%) = concentration at anode potential – concentration at OCV (1)

Formation rate (mol min^{-1}) = [(product concentration) × (gas flow rate)] / [standard state volume at SATP] (2)

Faradaic efficiency (%) = [(product formation rate) / (theoretical product formation rate)] × 100 (3)

The theoretical rate for methanol was calculated according to Faraday's law on the basis of the two-electron reaction.

3. Results and discussion

3.1. Characterization of lignosulfonate and anolyte

A SEM image and EDS spectra of the lignosulfonate used in the present study are shown in Fig. 1(a). The gray areas (B) and white areas (C) in the SEM image were somewhat unevenly distributed. The EDS analysis shows that the gray areas were rich in carbon, whereas the white areas were rich in Na and S. Carbon, oxygen, Na, and S accounted for 36.7, 36.6, 14.5, and 12.2 wt% of the composition of the total area (A), respectively. Lignosulfonates usually contain some amounts of carbonates as impurities [44]. We estimated the content of sodium carbonate (Na_2CO_3) to be 7.5 wt% in this sample by assuming that the sodium in excess to the sodium sulfonate groups (–SO_3Na, S:Na = 1:1) was Na_2CO_3. The Na_2CO_3 impurity is not believed to be involved in the oxidation reaction because, as will be shown later, the anode products did not contain Na.

Fig. 1(b) shows ^{1}H and ^{13}C NMR spectra of the lignosulfonate; signals of methoxy groups are observed at 3.5–4.0 ppm in the ^{1}H spectrum and at 56 ppm in the ^{13}C spectrum, along with signals of C–H in syringyl S, guaiacyl G, and *p*-hydroxyphenyl H units at 6.5–7.5 ppm in the ^{1}H

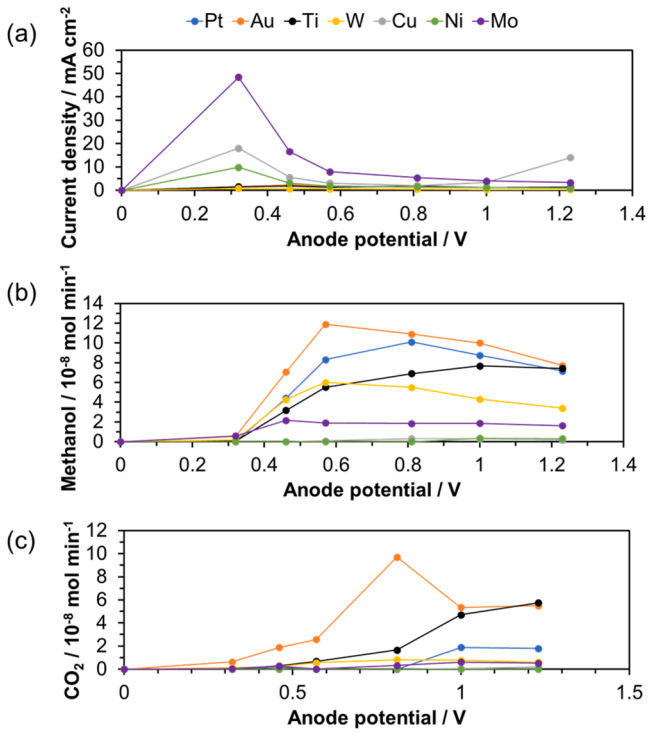

Fig. 2. (a) Current density, (b) methanol formation rate, and (c) CO_2 formation rate in the potential range zero–1.23 V. The electrolysis conditions were set as follows: lignosulfonate = 10 mg; 85% H_3PO_4 = 30 mg; temperature = 75 °C; He flow rate = 5 mL min^{-1}. All data were recorded at 5 min after the start of electrolysis.

spectrum and at 100–120 ppm in the ^{13}C spectrum [45,46]. In addition, the ^{13}C NMR spectrum shows signals assigned to C_γ–H_γ, C_β–H_β, and C_α–H_α at 60, 65, and 70 ppm, respectively, aromatic C═C and C–O at 120–140 and 150 ppm, respectively, and C═O in acetates at 190 ppm. Fig. 1(c) shows an FT-IR spectrum of the lignosulfonate. The observed absorption bands are attributable to O–H stretching (3200–3700 cm^{-1}), C–H stretching of methyl groups (2840 and 2940 cm^{-1}), aromatic skeletal vibrations (1510 and 1595 cm^{-1}), C–H bending of methyl groups (1370 and 1450 cm^{-1}), and C–O stretching (1150 and 1270 cm^{-1}) [47].

In our previous study, lignosulfonate was scarcely oxidized even at 100 °C in a H_3PO_4 anolyte [39]; however, the lignosulfonate was substantially oxidized in an H_2SO_4 anolyte, accompanied by the generation of white smoke. In addition, a mixture of lignosulfonate and H_3PO_4 was still in the liquid state at 100 °C when mixed at a ratio of 1:2.8. Thus, H_3PO_4 was used as an anolyte for the electrolysis in the present study. For a mixture of lignosulfonate and H_3PO_4 (weight ratio of 1:3), no peaks were observed outside the absorption bands of the respective components in the FT-IR spectra (Fig. 1(c)), indicating that the reaction of these components was negligible, at least at room temperature. TG–DTA curves for the lignosulfonate, H_3PO_4, and the mixture were recorded with the samples under Ar. As shown in Fig. 1(d), the lignosulfonate released water equivalent to 4.5 wt% of its total weight and began to undergo pyrolysis at approximately 200 °C. Dehydration of H_3PO_4 continued even above 100 °C. By contrast, the mixture underwent an endothermic reaction at 142 °C apart from dehydration. Thus, the electrolysis should be conducted below this temperature to prevent secondary reactions.

3.2. *Optimization of anode catalyst for electrolysis of lignosulfonate*

Various metal meshes were used as anodes to oxidize the

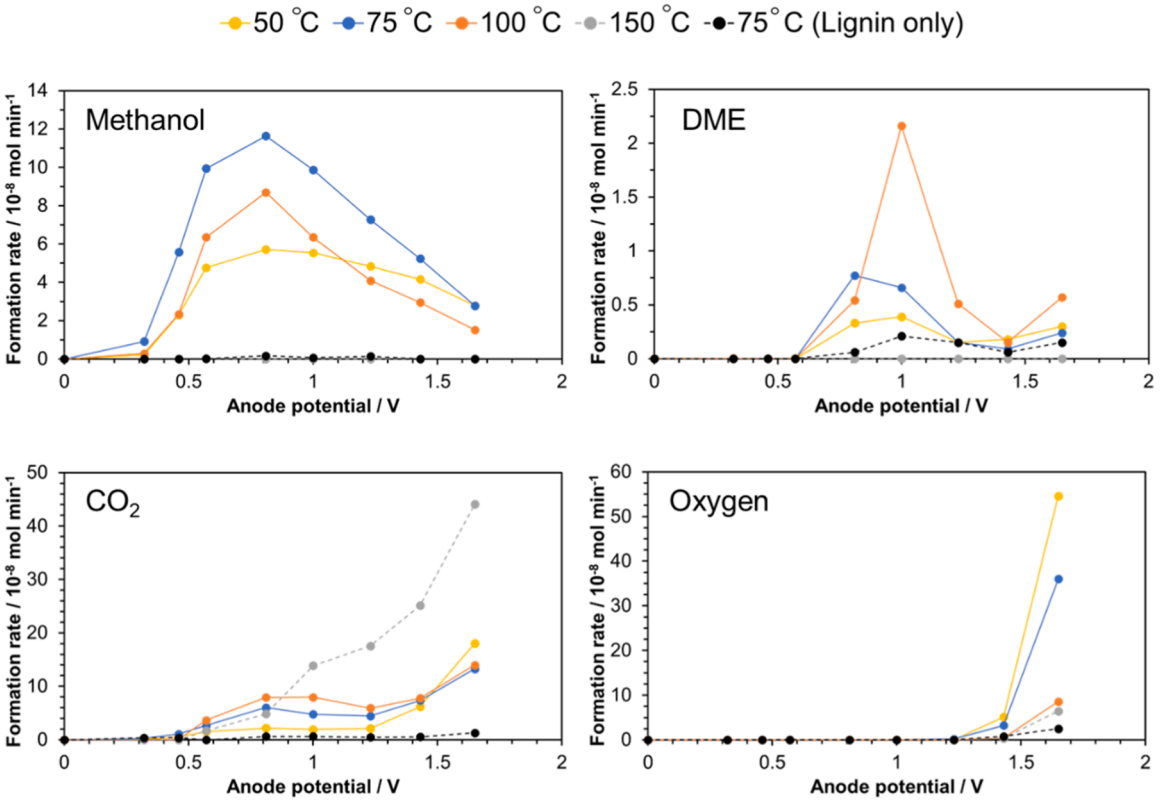

Fig. 3. Methanol (upper left), DME (upper right), CO_2 (lower left), and oxygen (lower right) were observed as gaseous products. The electrolysis was conducted in the potential range zero–1.65 V and in the temperature range 50–150 °C. The lignosulfonate (10 mg) was mixed with 30 mg of 85% H_3PO_4. All data were recorded at 5 min after the start of electrolysis. Data for the electrolysis of lignosulfonate alone at 75 °C are included for comparison.

lignosulfonate. Electrolysis characteristics were assessed in the H_3PO_4 anolyte with 10 mg of lignosulfonate at 75 °C. The results recorded at 5 min after the start of electrolysis at each anode potential are shown in Fig. 2. Upon anodic polarization, the current density varied depending on the anode species (Fig. 2(a)). Especially at +0.32 V, the Mo, Cu, and Ni anodes exhibited extremely high current densities compared with the other anodes. The redox potentials of these metals are Ti^{2+}/Ti −1.63 V; Ni^{2+}/Ni −0.25 V; Mo^{3+}/Mo −0.20 V; W^{6+}/W −0.09 V; Cu^{2+}/Cu +0.34 V; Pt^{2+}/Pt +1.18 V; and Au^{3+}/Au +1.50 V. In the absence of strong reducing power of the lignosulfonate, Ti, Ni, Mo, W, and Cu would be oxidized by anodic polarization; however, Ti and W showed low corrosion current densities because of the growth of a passivation film [48] and a high-electrical-resistance layer [49], respectively. Methanol, DME, and carbon dioxide (CO_2) were detected as products for all the tested anodes. Au, Pt, Ti, and W showed relatively high activity toward lignosulfonate oxidation (Fig. 2(b) and (c)), which suggests that high corrosion resistance is important for this electrolysis. The catalytic comparison indicates that Au provided the highest methanol and CO_2 formation rates over a wide range of potentials. By contrast, Pt was inferior to Au in methanol formation but considerably suppressed CO_2 formation.

We next attempted to modify the electrocatalytic activity of the Pt anode by sputtering metal particles onto the surface of the electrolyte. The mass of Pt on the anode was adjusted through modification of the sputtering time: 0.05, 0.12, 0.21, and 0.24 mg cm^{-2} of Pt were obtained for sputtering times of 10, 20, 30, and 40 min, respectively. The area-specific ohmic resistance decreased with increasing Pt mass, resulting in values of 7.6, 5.0, 3.4, and 3.3 Ω cm^2. This effect is attributable to an improvement in the current collection of the anode; therefore, the optimal sputtering time was determined to be 30 min. The average size of Pt crystallites estimated from the XRD patterns was 7 nm (Fig. S2), and a cross-sectional SEM image showed that these crystallites were deposited onto the electrolyte surface with a thickness of ~150 nm (Fig. S3). Hirano et al. have reported a similar relationship between the Pt loading, crystallite size, and thickness [50].

The effects of the sputtering of Pt appear in the impedance spectra of the cell at OCV and in the current–time curves under anodic polarization. The ohmic resistance at the electrode–electrolyte interface was reduced by one-half, and the capacitive reactance observed at low-to-medium frequencies increased (Fig. S4). These results indicate that the sputtering of Pt substantially increased the geometrical area of the electrode. As a result, the use of a sputtered Pt anode increased the current density under a constant potential (e.g., at +0.52 V) compared with the current density when a Pt mesh anode was used (Fig. S5).

3.3. Electrolysis of lignosulfonate to methanol over the sputtered Pt anode

The impedance spectra recorded at OCVs show two features: ohmic resistance that is almost independent of the temperature, and polarization resistance that decreases with increasing temperature (Fig. S6). However, the current density varies in a complicated manner with respect to the anode potential and temperature: small current-density peaks appeared at a potential of approximately +0.5 V, the current density increased considerably at potentials greater than +1.5 V, and a monotonic increase in the current density with potential was observed only at 150 °C (Fig. S7). The decrease in current density at +1.65 V with increasing temperature is attributed to the relative humidity (RH) of the humidified He carrier gas, as described later. Another important result is that the cell without the H_3PO_4 anolyte showed very low current densities because the insulating lignosulfonate disturbed the electrical collection on the anode.

Fig. 3 shows the gaseous product profiles for the electrolysis cell at various anode potentials and temperatures. Notably, as the potential increased, methanol, DME, CO_2, and oxygen were produced in that order. In addition, the highest formation rates were obtained at 75 °C for methanol, 100 °C for DME, 150 °C for CO_2, and 50 °C for oxygen.

Table 1
Gas compositions of the outlet gas over the range 50–125 °C under open-circuit conditions and at 75 °C under electrolysis conditions.

Temp. / °C	Potential / V	Current / mA cm^{-2}	Gas	Methanol / 10^{-7} mol	DME	CO_2
50	OCV	0	He+H_2O	0.03	> 0.01	0.04
75	OCV	0	He+H_2O	0.05	> 0.01	0.08
100	OCV	0	He+H_2O	0.19	0.01	0.16
125	OCV	0	He+H_2O	0.37	0.03	0.30
75	OCV	0	He+H_2O+O_2 (O_2 0.22%)	0.11	> 0.01	0.07
75	+0.46	2.4	He+H_2O	0.55	> 0.01	0.10
75	+0.57	2.0	He+H_2O	0.99	> 0.01	0.26
75	+0.81	1.5	He+H_2O	1.21	0.07	0.60

The gas compositions of electrolysis products were recorded at 5 min after the start of potential application.

Almost no gas was generated from pure lignosulfonate. Note also that the methanol formation rates at 75 °C were higher than those of the cell with the Pt mesh anode over all of the tested potential ranges (Fig. 2 vs. Fig. 3). Taken together with the aforementioned current–voltage curves (see Fig. S7), these results show that the electrochemical reactions of lignosulfonate proceed as follows: electro-oxidation of lignosulfonate begins at approximately +0.3 V to produce methanol; some of the methanol is dehydrated to DME and oxidized to CO_2 at higher potentials; the oxygen evolution reaction (OER) proceeds above +1.5 V; and the over-oxidation of lignosulfonate to CO_2 occurs from approximately +0.5 V only at 150 °C. In these measurements, because the P_{H2O} of the humidified He was constant at 0.002 MPa, the RHs at 50, 75, 100, and 150 °C were 27%, 5%, 2%, and 0.5%, respectively. In water-vapor electrolysis, when the RH is constant at each temperature, the current density increases with increasing temperature [51]. By contrast, as the RH decreases with increasing temperature, the OER overvoltage increases, resulting in a decrease in current density [52], which is consistent with the results for current density (Fig. S7) and the resultant oxygen formation rate (Fig. 3) at +1.65 V. However, at 150 °C, the reactivity of lignosulfonate is high and the anodic overvoltage is thought to remain exceptionally low.

The reaction of lignosulfonate with oxygen at the Pt anode is non-negligible. We investigated the thermocatalytic characteristics of the Pt anode by supplying a mixture of He, water vapor, and oxygen under open-circuit conditions. As shown in Table 1, very small amounts of methanol, DME, and CO_2 were generated in the substantial absence of oxygen at OCVs, and these amounts increased with increasing temperature. The formation of these gases was likely due to thermal decomposition or hydrolysis of the lignosulfonate. Table 1 also shows that the formation of methanol was enhanced in the presence of 0.22% oxygen, which is comparable to the oxygen amount electrochemically generated at a current density of 6.5 mA cm^{-2}. However, markedly larger enhancement effects were observed when the anode was polarized at +0.46, +0.57, and +0.81 V, although not only methanol production but also DME and CO_2 production was promoted. These results indicate that, compared with gas-phase oxygen, the electrochemically generated oxygen species is more active for the lignosulfonate oxidation. Recent advances in the generation of active oxygen species and the effectiveness of the species in electrochemical reactions have been reviewed by Shi et al. [53].

3.4. Continuous methanol extraction from lignosulfonate in the electrolysis cell

The aforementioned results are characteristics corresponding to 5 min after the start of electrolysis at each potential and temperature. To better understand the performance and kinetics of electrolysis, we conducted continuous electrolysis of lignosulfonates under various conditions. First, the amounts of extraction or oxidation products during

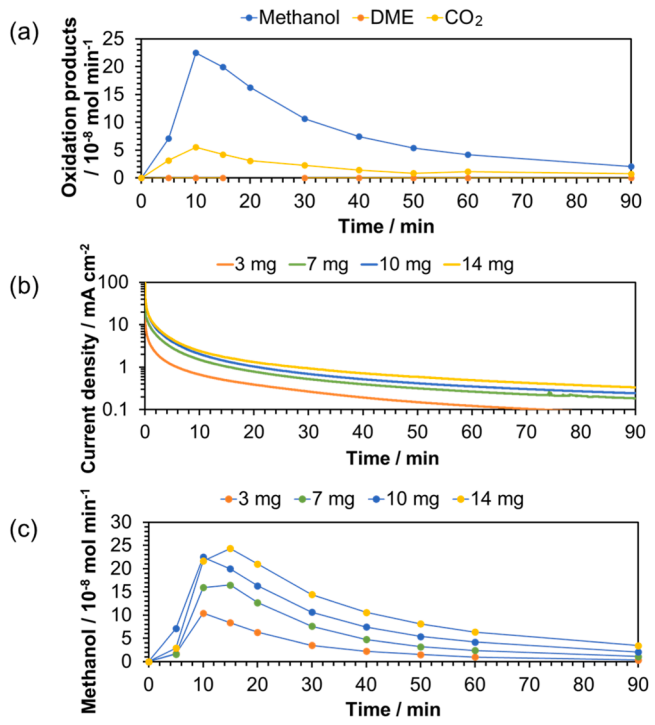

Fig. 4. Changes in (a) formation rate for oxidation products during electrolysis of 10 mg of lignosulfonate and (b) current density and (c) methanol formation rate during electrolysis of various weights of lignosulfonate with time. Conditions: temperature = 75 °C; anode potential = +0.57 V; lignosulfonate:85% H_3PO_4 = 1:3; He flow rate = 5 mL min^{-1}. Although the graphs only show data to 90 min, all experiments were continued until no methanol was produced.

continuous electrolysis of 10 mg lignosulfonate were measured at an anode potential of +0.57 V and a temperature of 75 °C. As shown in Fig. 4(a), the major products were methanol and CO_2. Note also that the product amounts reached maxima at 10 min after the start of electrolysis and then decreased substantially over time. This behavior is attributed to the current density decreasing from 4.23 to 0.24 mA cm^{-2} over time (blue line in Fig. 4(b)). Fig. 4(c) shows the methanol extraction when various weights of lignosulfonate were used under the same conditions. The amount of methanol at each time increased with increasing amount of lignosulfonate, which corresponds well to the increase in current density at that time (orange, green, blue, and yellow lines in Fig. 4(b)).

We next calculated the rate constants for the lignosulfonate oxidation reaction and the subsequent methanol oxidation reaction by assuming the following reaction rate equations:

$$d[\text{Methoxy group}]/dt = -k_1[\text{Methoxy group}][O] \quad (4)$$

$$d[\text{Methanol}]/dt = k_1[\text{Methoxy group}][O] - k_2[\text{Methanol}][O] \quad (5)$$

$$d[CO_2]/dt = k_2[\text{Methanol}][O] \quad (6)$$

where [*Methoxy group*] is the concentration (number of moles) of methoxy groups in the lignosulfonate. In this case, the initial value was determined by this content being 8.7 wt% of the lignosulfonate; the value at time *t* was obtained by subtracting the total number of moles of products (methanol, DME, and CO_2) at each time from the initial value. [*O*] is the concentration (number of moles) of oxygen species produced via the two-electron reaction:

$$H_2O \rightarrow O + 2H^+ + 2e^- \quad (7)$$

Fig. 5(a)–(d) shows the dependence of the reaction rates on the concentration of each reactant for the lignosulfonate oxidation represented in Fig. 4. Characteristically, the formation rate of CO_2 was proportional to the methanol and oxygen concentrations, respectively,

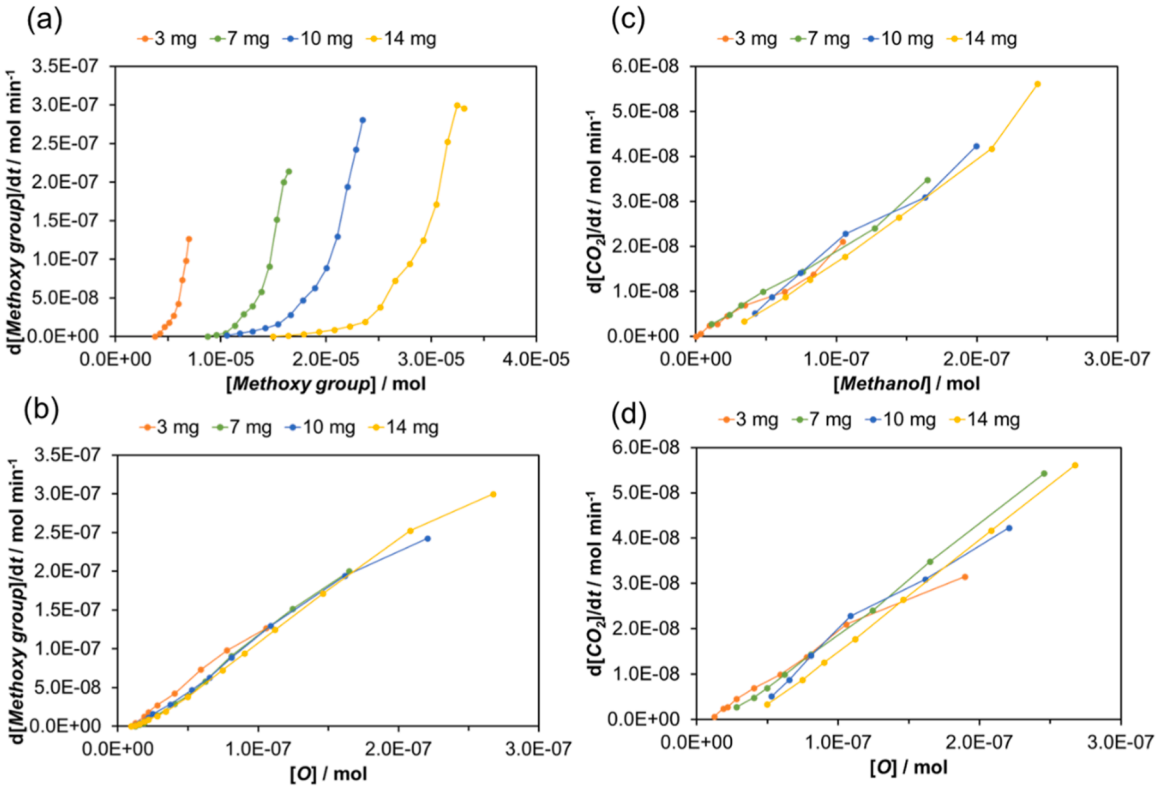

Fig. 5. Dependences of the lignosulfonate oxidation rate on (a) the methoxy-group concentration and (b) the oxygen-species concentration, and dependences of the methanol oxidation rate on (c) the methanol concentration and (d) the oxygen-species concentration. Experimental conditions are the same as those specified in Fig. 4.

Table 2
Rate constants for sequential reactions under various conditions.

Rate constant	$k_1 \times 10^{-5}$ / mol^{-1} min^{-1}	$k_2 \times 10^{-5}$ / mol^{-1} min^{-1}
Anode potential / V[a]		
0.32	0.38	4.88
0.57	0.57	8.34
0.81	0.64	10.9
Temperature / °C[b]		
50	0.46	3.94
75	0.57	8.34
100	0.50	15.4

[a] Conditions: lignosulfonate = 10 mg; temperature = 75 °C.
[b] Conditions: lignosulfonate = 10 mg; anode potential = +0.57 V.

according to Eq. (6), whereas the oxidation rate of lignosulfonate was proportional to the oxygen concentration but independent of the methoxy-group concentration. Therefore, the lignosulfonate can be considered to be oxidized according to a pseudo-first-order reaction equation that is proportional only to the oxygen concentration, which reflects either the excess amount of methoxy groups relative to the amount of oxygen species or an extremely lower reactivity of the lignosulfonate compared with that of the oxygen species.

The reaction rates represented by Eqs. (4) and (6) were also dependent on the anode potential and temperature (Fig. S8). The rate constants obtained from these slopes are summarized in Table 2. Rate constant k_2 was greater than rate constant k_1 at all of the tested potentials and temperatures, indicating that methanol is more easily oxidized than lignosulfonate. Because k_2 decreased with decreasing potential and temperature, the selectivity toward methanol was improved under such conditions. However, the potential of +0.32 V and temperature of 50 °C are not favorable conditions for oxidation of the lignosulfonate because the k_1 values corresponding to these conditions are low. We thus determined that the optimal anode potential and temperature for methanol extraction from lignosulfonate are +0.57 V and 75 °C, respectively.

Under the aforementioned conditions, continuous electrolysis was conducted until methanol production ceased. The total amounts of methanol extracted from the lignosulfonate were subsequently calculated by integrating the areas under the formation rate–time curves, respectively. A linear relationship was observed between the methanol weight and the lignosulfonate weight (Fig. S9(a)). The amounts of methanol obtained for 3, 7, 10, and 14 mg of lignosulfonate correspond to 3.1, 2.8, 3.3, and 3.1 wt% of the amount of the dry feedstock, respectively. Because the lignosulfonate used in the experiments contained 14.5 wt% Na, the aforementioned methanol amounts were corrected to 3.7, 3.3, 3.8, and 3.6 wt% per weight of feedstock excluding Na. On the basis of the reported content (8.7 wt%) of methoxy groups in lignosulfonate [24], the methanol yield was calculated to be an average of 41.5%.

The faradaic efficiency for methanol formation was also calculated on the basis of the two-electron reaction. Maximum efficiencies of 90–95% were obtained for 3–14 mg lignosulfonate during the first 15–20 min of electrolysis (Fig. S9(b)). As the reaction progressed, a higher efficiency was maintained for larger amounts of lignosulfonate. A distinctive feature of the faradaic efficiency is that its value decreased over time, irrespective of the lignosulfonate weight. This trend can be attributed to two causes: first, the faradaic efficiency for CO_2 formation increased with time; second, the anode potential was as low as +0.57 V. Thus, the lower the current density, the higher the proportion of nonfaradaic current due to the electrical double layer. As an example, the current density was measured to be 0.24 mA cm^{-2} at a reaction time of 90 min, where methanol and CO_2 were produced with efficiencies of 50% and 40%, respectively, with no other detectable gases. Therefore, the nonfaradaic current density was estimated to be 0.02 mA cm^{-2}, which corresponds to 10% of the aforementioned current density. The proportion of nonfaradaic current density gradually increased with increasing reaction time.

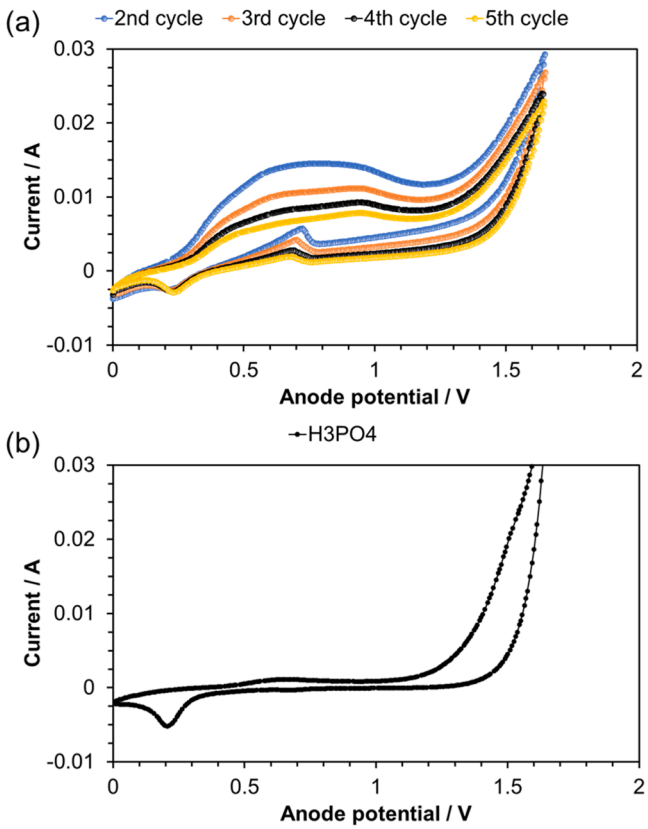

Fig. 6. (a) CV curves with 10 mg of lignosulfonate on the anode and (b) CV curve without lignosulfonate. Conditions: temperature = 75 °C; He flow rate = 5 mL min^{-1}; air flow rate at the cathode = 5 mL min^{-1}; scan rate = 50 mV s^{-1}.

Continuous flow reactors can contribute to solving the problems specific to lignosulfonate in the unstirred batch operation because they enable the amount of available lignosulfonate to be adjusted while balancing the yield and efficiency [40,54,55]. We have previously demonstrated a method for continuous electrolysis by supplying a mixture of biomass waste and H_3PO_4 to the anode at a constant rate using a syringe pump [43]. Although the supply time was limited to 6000 s because of the volume of the syringe container, we confirmed that the cell operated stably during the experiment for all of the biomass tested. Notably, this stability was achieved at an operation temperature of 175 °C, which is much higher than the operation temperature of 75 °C used in the present study. However, the liquid flow method requires the products to be fractionated from the effluent mixture before recirculation. DME and CO_2 have low boiling points of −24 °C and −78 °C, respectively; therefore, they evaporate at room temperature. Methanol can then be recovered by heating the effluent above its boiling point of 65 °C.

3.5. Characterization of active species and reaction intermediates and residues

Characterization of the electrode surface, the catalytically active species, and the reaction residues in the anode is critical to elucidate the mechanism of the oxidation reaction. To gain additional insight into the electro-oxidation of lignosulfonate, cyclic voltammetry (CV) profiles were recorded over the potential range from zero to +1.6 V. The CV curves show a broad oxidation peak between +0.25 and +1.15 V, the peak value of which decreased with increasing number of scans (Fig. 6 (a)). By contrast, no such peak appeared in the absence of lignosulfonate

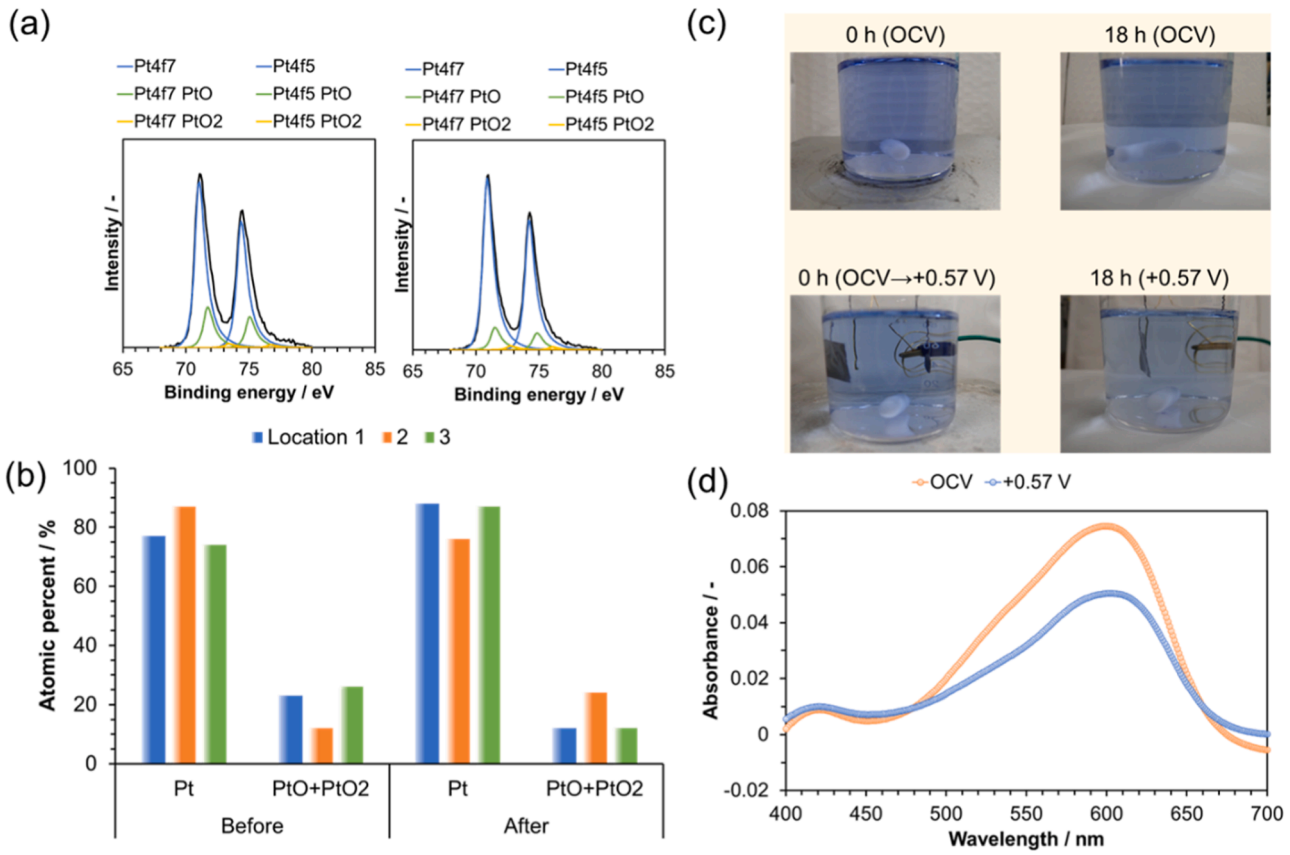

Fig. 7. (a) Deconvoluted XPS Pt 4*f* spectra and (b) elemental compositions of the electrode surface measured at different locations for a Pt anode before and after electrolysis. (c) Color change of methyl violet solution and (d) change in the UV–vis absorbance of methyl violet in the solution as a result of water electrolysis for 18 h. The water electrolysis was performed at an anode potential of +0.57 V and room temperature. Images and UV–vis absorbance without polarization are included for comparison.

(Fig. 6(b)). This peak is thus reasonably assigned to the oxidation of lignosulfonate to methanol and then to DME and CO_2. More importantly, a small oxidation peak was observed at a potential of approximately +0.7 V in the reverse scan when lignosulfonate was present, indicating that the oxidation of lignosulfonate was resumed when the scan direction was reversed. These results suggest that this oxidation reaction proceeds through the formation of active species or a reaction initiator and that the reactivity of these species is strongly influenced by the anode potential [56–58]. Presumably, these species can undergo proton withdrawal in the forward-direction scan and proton insertion in the reverse-direction scan.

The oxidation state of Pt in the anode before and after electrolysis at +0.57 V was compared through deconvolution of the Pt 4*f* signal in the XPS spectra acquired at three different locations on the anode surface. Both the Pt 4*f* signals before and after electrolysis were assigned to three components indexed to Pt, PtO, and PtO_2 (Fig. 7(a)). The atomic percentages of each component before and after electrolysis were similar when averaged over different locations (Fig. 7(b)). Therefore, metallic Pt atoms are not oxidized to high valence states by the anodic polarization at +0.57 V, which suggests that the active species or reaction initiators are weakly bound to Pt atoms or chemisorbed to its surface. Hydroxyl radicals have been reported to play an important role as an active oxidant in various anodic reactions [59–61]. To clarify whether $^{\bullet}$OH radicals are formed from water molecules at the anode, we electrolyzed water using the Pt anode in a solution containing methyl violet because this compound becomes colorless upon reacting with $^{\bullet}$OH radicals [62]. Compared with the violet color of the reference cell maintained at the OCV for 18 h, the color of the solution in the cell became weaker after electrolysis for the same time (Fig. 7(c)). The UV–vis absorbance spectrum of the solution in the electrolysis cell also showed a smaller peak at 604 nm (corresponding to absorption by methyl violet) compared with the spectrum of the solution in the reference cell (Fig. 7(d)). In previous studies, the generation of $^{\bullet}$OH radicals over Pt anodes through water oxidation has been confirmed by other techniques, including UV–vis absorbances of *N*,*N*-dimethyl-*p*-nitrosoaniline [63] and salicylic acid [64], optical emission spectroscopy [65], and electron-spin resonance spectroscopy [66]. We can thus assume that $^{\bullet}$OH radicals function as an active species for lignosulfonate oxidation.

The lignin residue after electrolysis was characterized by FT-IR spectroscopy. The C–O stretching peaks (1150 and 1270 cm^{-1}), CH_3 bending peaks (1370 and 1450 cm^{-1}), and CH_3 stretching peaks (2840 and 2940 cm^{-1}) almost disappeared from the FT-IR spectrum of the residue (Fig. 8(a)). Similarly, the NMR spectrum shows that the integrated intensity of the methoxy group signal at 3.6 ppm decreased by a factor of 9 after electrolysis (Fig. 8(b)). These results imply that most of the methoxy groups in the lignosulfonate were demethylated. Indeed, few components containing methoxy groups were detected by GC–MS analysis of the residues dissolved in a methanol solvent (Fig. 8(c)); peaks observed at ~2 min in the chromatogram were attributed to sulfur dioxide, column bleed components, and hydrochloric acid. As optional information, when the CV measurement of lignosulfonate was continued for more than five scans, a reduction peak began to appear at approximately +0.7 V, along with a decrease in intensity of the oxidation peak, with increasing scan number (Fig. S10). This peak is not assigned to a Pt^{2+}/Pt or Pt^{+}/Pt reduction reaction because it was not observed in the CV curve for the system without lignosulfonate; thus, some components of the residue exhibit redox activity.

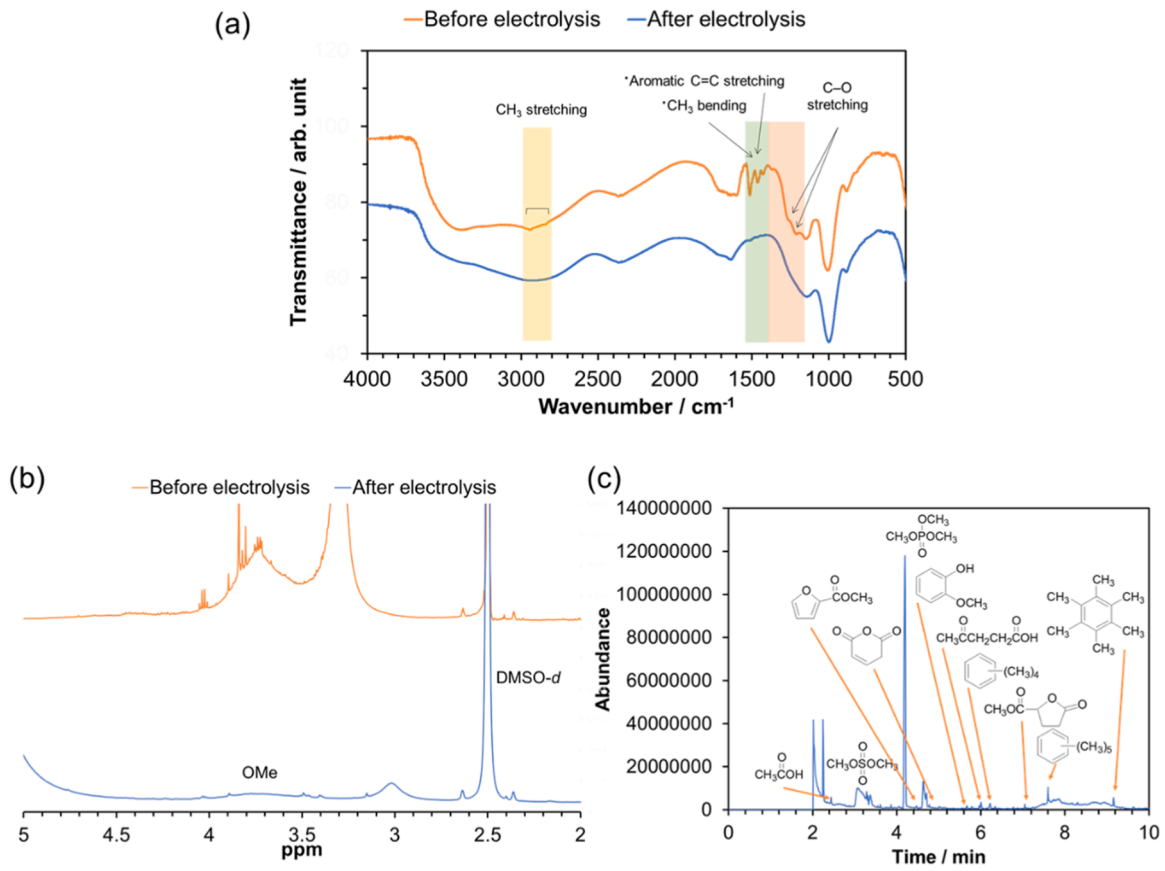

Fig. 8. (a) FT-IR and (b) ^{1}H NMR spectra of lignosulfonate before and after electrolysis. (c) GC–MS chromatogram of lignosulfonate residue dissolved in methanol after electrolysis. The residue was obtained by the continuous electrolysis shown in Fig. 4. The intensity of the NMR spectra was normalized according to the intensity of DMSO-d_6. The residue was further dissolved in methanol, centrifuged, and collected as the supernatant liquid for the GC–MS measurement.

3.6. Reaction mechanism for the electrochemical demethylation of lignosulfonate

On the basis of the aforementioned observations and similar reports in the literature [29,67–69], we propose the following reaction scheme for the electrochemical extraction of methanol from lignosulfonate (Fig. S11). First, the formation of •OH radicals from water proceeds over the anode. In the second stage, this radical reacts with a hydroxyl group of lignosulfonate to form a phenoxy radical accompanied by a conjugated form. In the third stage, the conjugated form generates a hemiketal bond with a •OH radical. Finally, the hemiketal is converted into methanol and a quinone. Part of the methanol is dehydrated to DME and oxidized to CO_2. Moreover, the GC–MS results suggested that some of the quinone is further converted electrochemically or catalytically to ring-retaining and ring-opening products. Other byproducts observed were trimethyl phosphate [$(CH_3O)_3PO$] and dimethyl sulfate [$(CH_3O)_2SO_2$]. These compounds are thought to be formed as follows:

$$H_3PO_4 + 3CH_3OH \rightarrow (CH_3O)_3PO + 3H_2O \quad (8)$$

$$R\text{–}SO_3Na + 2CH_3OH \rightarrow (CH_3O)_2SO_2 + R\text{–}OH \quad (9)$$

The formation of these compounds reduced the methanol yield. Apart from this oxidative route, lignin monomer model compounds such as 2-methoxy and 2,6-dimethoxy phenols have been reported to be demethoxylated to phenol and methanol according to a reductive route via the formation of hydrogen radicals during the hydrogen evolution reaction (HER) [34,70,71]. However, this route has not yet been demonstrated for lignin polymers.

At the cathode, hydrogen was evolved over the anode potential range from +0.3 to +1.6 V, whereas the cathode potential was constant at approximately −0.55 V (Fig. S12), implying that the amount of hydrogen produced depends only on the current density. Note also that the concentration of oxygen leaking into He from outside the cathode also decreased at +0.32 V or higher; therefore, some hydrogen reacted with impurity oxygen, which reduced the faradaic efficiency for the HER but suggests the progress of the ORR. Indeed, when air was supplied to the cathode instead of He, the cell generated an OCV of 0.45 V and a peak power density of 0.14 mW cm^{-2} (Fig. S13). Simultaneously, the generation of methanol from the lignosulfonate was confirmed through self-shorting of the fuel cell, although the formation rate of methanol was lower in the fuel cell than in the electrolysis cell because of its low short-circuit current (Fig. S14). Thus, the electro-oxidation reactions shown in Fig. S11 were demonstrated to occur also in fuel-cell mode. This fuel cell can be distinguished from other fuel cells that use lignin derivatives directly as fuels, where the anode product is a mixture of aromatic and aliphatic compounds [72–74].

4. Conclusions

We demonstrated a technology to use technical lignin as a resource for methanol. A notable feature of this technology is that methanol was extracted with a faradaic efficiency greater than 90% under conditions of atmospheric pressure, 75 °C, and a low overpotential. In addition, a methanol yield greater than 40% was achieved without stirring the reaction system or performing an extra separation operation. Furthermore, using a fuel-cell reactor could mitigate the energy required for the electrolysis process. These achievements are the result of successfully controlling the quantity and quality of reactive species through the synergistic effect of Pt catalytic activity and the anode potential.

CRediT authorship contribution statement

Takashi Hibino: Conceptualization, Supervision, Project administration, Funding acquisition, Writing – original draft. **Kazuyo Kobayashi:** Methodology, Investigation. **Dongwen Zhou:** Investigation. **Siyuan Chen:** Investigation. **Shinya Teranishi:** Investigation. **Aki Miyawaki:** Investigation. **Yoshiharu Sawada:** Investigation. **Anatoly Zinchenko:** Investigation.

Declaration of Competing Interest

The authors declare that they have no known competing financial interests or personal relationships that could have appeared to influence the work reported in this paper.

Data availability

Data will be made available on request.

Acknowledgments

This research was funded by a Kakenhi Grant-in-Aid (No. 17H01895) from the Japan Society for the Promotion of Science (JSPS), and by a grant (No. JPMJCR18R2) from the CREST Program of the Japan Science and Technology Agency (JST). This research was also the result of using research equipment shared in a MEXT Project for promoting public utilization of advanced research infrastructure (Program for supporting construction of core facilities) Grant Number JPMXS04411023.

Appendix A. Supporting information

Supplementary data associated with this article can be found in the online version at doi:10.1016/j.apcatb.2023.123328.

References

[1] J. Ralph, C. Lapierre, W. Boerjan, Lignin structure and its engineering, Curr. Opin. Biotechnol. 56 (2019) 240–249, https://doi.org/10.1016/j.copbio.2019.02.019.
[2] C. Heitner, D. Dimmel, J. Schmidt, Lignin and Lignans: Advances in Chemistry, CRC Press, Boca Raton, FL, 2016.
[3] C. Nitsos, R. Stoklosa, A. Karnaouri, D. Vörös, H. Lange, D. Hodge, C. Crestini, U. Rova, P. Christakopoulos, Isolation and characterization of organosolv and alkaline lignins from hardwood and softwood biomass, ACS Sustain. Chem. Eng. 4 (2016) 5181–5193, https://doi.org/10.1021/acssuschemeng.6b01205.
[4] Y. Zhang, M. Qin, W. Xu, Y. Fu, Z. Wang, Z. Li, S. Willför, C. Xu, Q. Hou, Structural changes of bamboo-derived lignin in an integrated process of autohydrolysis and formic acid inducing rapid delignification, Ind. Crop. Prod. 115 (2018) 194–201, https://doi.org/10.1016/j.indcrop.2018.02.025.
[5] A. Fujimoto, Y. Matsumoto, H.M. Chang, G. Meshitsuka, Quantitative evaluation of milling effects on lignin structure during the isolation process of milled wood lignin, J. Wood Sci. 51 (2005) 89–91, https://doi.org/10.1007/s10086-004-0682-7.
[6] S. Yang, T.-Q. Yuan, R.-C. Sun, Structural elucidation of whole lignin in cell walls of triploid of Populus tomentosa Carr, ACS Sustain. Chem. Eng. 4 (2016) 1006–1015, https://doi.org/10.1021/acssuschemeng.5b01075.
[7] B. Jiang, T. Cao, F. Gu, W. Wu, Y. Jin, Comparison of the structural characteristics of cellulolytic enzyme lignin preparations isolated from wheat straw stem and leaf, ACS Sustain. Chem. Eng. 5 (2017) 342–349, https://doi.org/10.1021/acssuschemeng.6b01710.
[8] R.G. Ferreira, A.R. Azzoni, S. Freitas, On the production cost of lignocellulose-degrading enzymes, Biofuels Bioprod. Biorefin. 15 (2021) 85–99, 10.1002/bbb.2142.
[9] H. Sadeghifar, A. Ragauskas, Perspective on technical lignin fractionation, ACS Sustain. Chem. Eng. 8 (2020) 8086–8101, https://doi.org/10.1021/acssuschemeng.0c01348.
[10] N.-E.El Mansouri, J. Salvadó, Structural characterization of technical lignins for the production of adhesives: application to lignosulfonate, kraft, soda-anthraquinone, organosolv and ethanol process lignins, Ind. Crop. Prod. 24 (2006) 8–16, https://doi.org/10.1016/j.indcrop.2005.10.002.
[11] T. Aro, P. Fatehi, Production and application of lignosulfonates and sulfonated lignin, ChemSusChem 10 (2017) 1861–1877, https://doi.org/10.1002/cssc.201700082.
[12] J. Ruwoldt, A critical review of the physicochemical properties of lignosulfonates: chemical structure and behavior in aqueous solution, at surfaces and interfaces, Surfaces 3 (2020) 622–648, https://doi.org/10.3390/surfaces3040042.
[13] S. Kang, X. Li, J. Fan, J. Chang, Hydrothermal conversion of lignin: a review, Renew. Sustain. Energy Rev. 27 (2013) 546–558, https://doi.org/10.1016/j.rser.2013.07.013.
[14] A.J. Ragauskas, et al., Lignin valorization: improving lignin processing in the biorefinery, Science 344 (2014), 1246843, https://doi.org/10.1126/science.1246843.
[15] D. Kai, M.J. Tan, P.L. Chee, Y.K. Chua, Y.L. Yap, X.J. Loh, Towards lignin-based functional materials in a sustainable world, Green Chem. 18 (2016) 1175–1200, https://doi.org/10.1039/C5GC02616D.
[16] L.A. Zevallos Torres, A. Lorenci Woiciechowski, V.O. de Andrade Tanobe, S. G. Karp, L.C. Guimarães Lorenci, C. Faulds, C.R. Soccol, Lignin as a potential source of high-added value compounds: a review, 121499–21516, J. Clean. Prod. 263 (2020), https://doi.org/10.1016/j.jclepro.2020.121499.
[17] W. Xie, J. Liang, H.M. Morgan Jr., X. Zhang, K. Wang, H. Mao, Q. Bu, Ex-situ catalytic microwave pyrolysis of lignin over Co/ZSM-5 to upgrade bio-oil, J. Anal. Appl. Pyrolysis 132 (2018) 163–170, https://doi.org/10.1016/j.jaap.2018.03.003.
[18] A. More, T.J. Elder, Z. Jiang, Towards a new understanding of the retro-aldol reaction for oxidative conversion of lignin to aromatic aldehydes and acids, Int. J. Biol. Macromol. 183 (2021) 1505–1513, https://doi.org/10.1016/j.ijbiomac.2021.05.100.
[19] R. Singh, A. Prakash, S.K. Dhiman, B. Balagurumurthy, A.K. Arora, S.K. Puri, T. Bhaskar, Hydrothermal conversion of lignin to substituted phenols and aromatic ethers, Bioresour. Technol. 165 (2014) 319–322, https://doi.org/10.1016/j.biortech.2014.02.076.
[20] J. Kang, S. Irmak, M. Wilkins, Conversion of lignin into renewable carboxylic acid compounds by advanced oxidation processes, Renew. Energy 135 (2019) 951–962, https://doi.org/10.1016/j.renene.2018.12.076.
[21] L. Kong, L. Zhang, J. Gu, L. Gou, L. Xie, Y. Wang, L. Dai, Catalytic hydrotreatment of kraft lignin into aromatic alcohols over nickel-rhenium supported on niobium oxide catalyst, Bioresour. Technol. 299 (2020), 122582, https://doi.org/10.1016/j.biortech.2019.122582.
[22] T. Han, W. Yang, P.G. Jönsson, Pyrolysis and subsequent steam gasification of metal dry impregnated lignin for the production of H_2-rich syngas and magnetic activated carbon, Chem. Eng. J. 394 (2020), 124902, https://doi.org/10.1016/j.cej.2020.124902.
[23] K.V. Sarkanen, C.H. Ludwig, Lignins: Occurence, Formation, Structure and Aeactions, Wiley-Interscience, New York, 1971, pp. 19–38.
[24] N.-E.E. Mansouri, J. Salvadó, Structural characterization of technical lignins for the production of adhesives: application to lignosulfonate, kraft, soda-anthraquinone, organosolv and ethanol process lignins, Ind. Crop. Prod. 24 (2006) 8–16, https://doi.org/10.1016/j.indcrop.2005.10.002.
[25] Z. Li, E. Sutandar, T. Goihl, X. Zhang, X. Pan, Cleavage of ethers and demethylation of lignin in acidic concentrated lithium bromide (ACLB) solution, Green Chem. 22 (2020) 7989–8001, https://doi.org/10.1039/d0gc02581j.
[26] X. Jiang, D. Savithri, X. Du, S.N. Pawar, H. Jameel, H. Chang, X. Zhou, Fractionation and characterization of kraft lignin by sequential precipitation with various organic solvents, ACS Sustain. Chem. Eng. 5 (2017) 835–842, https://doi.org/10.1021/acssuschemeng.6b02174.
[27] Q. Liu, T. Kawai, Y. Inukai, D. Aoki, Z. Feng, Y. Xiao, K. Fukushima, X. Lin, W. Shi, W. Busch, Y. Matsushita, B. Li, A lignin-derived material improves plant nutrient bioavailability and growth through its metal chelating capacity, Nat. Commun. 14 (2023), 4866, https://doi.org/10.1038/s41467-023-40497-2.
[28] Q. Mei, H. Liu, X. Shen, Q. Meng, H. Liu, J. Xiang, B. Han, Selective utilization of the methoxy group in lignin to produce acetic acid, Angew. Chem. Int. Ed. 56 (2017) 14868–14872, https://doi.org/10.1002/anie.201706846.
[29] E. Adler, S. Hernestam, Estimation of phenolic hydroxyl groups in lignin. I. Periodate oxidation of guaiacol compounds, Acta Chem. Scand. 9 (1955) 319–334.
[30] B. Venkatesagowda, R.F.H. Dekker, Microbial demethylation of lignin: evidence of enzymes participating in the removal of methyl/methoxyl groups, Enzym. Microb. Technol. 147 (2021), 109780, https://doi.org/10.1016/j.enzmictec.2021.109780.
[31] I. Bosque, G. Magallanes, M. Rigoulet, M.D. Karkas, C.R.J. Stephenson, Redox catalysis facilitates lignin depolymerization, ACS Cent. Sci. 3 (2017) 621–628, https://doi.org/10.1021/acscentsci.7b00140.
[32] X. Wu, X. Fan, S. Xie, J. Lin, J. Cheng, Q. Zhang, L. Chen, Y. Wang, Solar energy-driven lignin-first approach to full utilization of lignocellulosic biomass under mild conditions, Nat. Catal. 1 (2018) 772–780, https://doi.org/10.1038/s41929-018-0148-8.
[33] M. Garedew, F. Lin, B. Song, T.M. DeWinter, J.E. Jackson, C.M. Saffron, C.H. Lam, P.T. Anastas, Greener routes to biomass waste valorization: lignin transformation through electrocatalysis for renewable chemicals and fuels production, ChemSusChem 13 (2020) 4214–4237, https://doi.org/10.1002/cssc.202000987.
[34] M. Garedew, C.H. Lam, L. Petitjean, S. Huang, B. Song, F. Lin, J.E. Jackson, C. M. Saffron, P.T. Anastas, Electrochemical upgrading of depolymerized lignin: a review of model compound studies, Green Chem. 23 (2021) 2868–2899, https://doi.org/10.1039/D0GC04127K.
[35] D. Gao, D. Ouyang, X. Zhao, Electro-oxidative depolymerization of lignin for production of value-added chemicals, Green Chem. 24 (2022) 8585–8605, https://doi.org/10.1039/D2GC02660K.
[36] B. Jacobs, Y. Yao, I. Van Nieuwenhove, D. Sharma, G.J. Graulus, K. Bernaerts, A. Verberckmoes, Sustainable lignin modifications and processing methods: green chemistry as the way forward, Green Chem. 25 (2023) 2042–2086.
[37] J. Klein, R. Kupec, M. Stöckl, S.R. Waldvogel, Degradation of lignosulfonate to vanillic acid using ferrate, Adv. Sustain. Syst. 7 (2022), 2200431, https://doi.org/10.1002/adsu.202200431.

[38] D. Di Marino, D. Stöckmann, S. Kriescher, S. Stiefel, M. Wessling, Electrochemical depolymerisation of lignin in a deep eutectic solvent, Green Chem. 18 (2016) 6021–6028, https://doi.org/10.1039/C6GC01353H.
[39] T. Hibino, K. Kobayashi, M. Nagao, S. Teranishi, Hydrogen production by direct lignin electrolysis at intermediate temperatures, ChemElectroChem 4 (2017) 3032–3036, https://doi.org/10.1002/celc.201700917.
[40] A. Caravaca, W.E. Garcia-Lorefice, S. Gil, A. de Lucas-Consuegra, P. Vernoux, Towards a sustainable technology for H_2 production: direct lignin electrolysis in a continuous-flow polymer electrolyte membrane reactor, Electrochem. Commun. 100 (2019) 43–47, https://doi.org/10.1016/j.elecom.2019.01.016.
[41] H. Zhao, D. Lu, J. Wang, W. Tu, D. Wu, S.W. Koh, P. Gao, Z.J. Xu, S. Deng, Y. Zhou, B. You, H. Li, Raw biomass electroreforming coupled to green hydrogen generation, Nat. Commun. 12 (2021), 2008, https://doi.org/10.1038/s41467-021-22250-9.
[42] K. Shen, S. Kumari, Y.C. Huang, J. Jang, P. Sautet, C.G. Morales-Guio, Electrochemical oxidation of methane to methanol on electrodeposited transition metal oxides, J. Am. Chem. Soc. 145 (2023) 6927–6943, https://doi.org/10.1021/jacs.3c00441.
[43] T. Hibino, K. Kobayashi, M. Ito, M. Nagao, M. Fukui, S. Teranishi, Direct electrolysis of waste newspaper for sustainable hydrogen production: an oxygen-functionalized porous carbon anode, Appl. Catal. B Environ. 231 (2018) 191–199, https://doi.org/10.1016/j.apcatb.2018.03.021.
[44] O. Musl, I. Sulaeva, I. Sumerskii, A.K. Mahler, T. Rosenau, J. Falkenhagen, A. Potthast, ACS Sustain. Chem. Eng. 9 (2021) 16786–16795, https://doi.org/10.1021/acssuschemeng.1c06469.
[45] Y. Qian, Q. Zhang, X. Qiu, S. Zhu, CO_2-responsive diethylaminoethyl-modified lignin nanoparticles and their application as surfactants for CO_2/N_2-switchable Pickering emulsions, Green Chem. 16 (2014) 4963–4968, https://doi.org/10.1039/C4GC01242A.
[46] K. Bahrpaima, P. Fatehi, Preparation and coagulation performance of carboxypropylated and carboxypentylated lignosulfonates for dye removal, Biomolecules 9 (2019) 383, https://doi.org/10.3390/biom9080383.
[47] H. Mainka, L. Hilfert, S. Busse, F. Edelmann, E. Haak, A.S. Herrmann, Characterization of the major reactions during conversion of lignin to carbon fiber, J. Mater. Res. Technol. 4 (2015) 377–391, https://doi.org/10.1016/j.jmrt.2015.04.005.
[48] A. Sawa, Resistive switching in transition metal oxides, Mater. Today 11 (2008) 28–36, https://doi.org/10.1016/S1369-7021(08)70119-6.
[49] M.I. Nave, G.K. Konstantin, Complexity of products of tungsten corrosion: comparison of the 3D Pourbaix diagrams with the experimental data, Metall. Mater. Trans. A 48 (2017) 1414–1424, https://doi.org/10.1007/s11661-016-3888-6.
[50] S. Hirano, J. Kim, S. Srinivasan, High performance proton exchange membrane fuel cells with sputter-deposited Pt layer electrodes, Electrochim. Acta 42 (1997) 1587–1593, https://doi.org/10.1016/S0013-4686(96)00320-9.
[51] S. Sawada, T. Yamaki, T. Maeno, M. Asano, A. Suzuki, T. Terai, Y. Maekawa, Solid polymer electrolyte water electrolysis systems for hydrogen production based on our newly developed membranes, part I: analysis of voltage–current characteristics, Prog. Nucl. Energy 50 (2008) 443–448, https://doi.org/10.1016/j.pnucene.2007.11.029.
[52] J.C. Fornaciari, M.R. Gerhardt, J. Zhou, Y.N. Regmi, N. Danilovic, A.T. Bell, A. Z. Weber, The role of water in vapor-fed proton-exchange-membrane electrolysis, J. Electrochem. Soc. 167 (2020), 104508, https://doi.org/10.1149/1945-7111/ab9b09.
[53] T. Shi, D. Sridhar, L. Zeng, A. Chen, Recent advances in catalyst design for the electrochemical and photoelectrochemical conversion of methane to value-added products, Electrochem. Commun. 135 (2022), 107220, https://doi.org/10.1016/j.elecom.2022.107220.
[54] M. Khalid, B.S. De, A. Singh, S. Shahgaldi, Lignin electrolysis at room temperature on nickel Foam for hydrogen generation: performance evaluation and effect of flow rate, Catalysts 12 (2022) 1646, https://doi.org/10.3390/catal12121646.
[55] J.-E. Rodríguez-Fernández, M. Rojo, J.R. Avilés-Moreno, P. Ocón, Clean H_2 production by lignin-assisted electrolysis in a polymer electrolyte membrane flow reactor, Materials 16 (2023) 3525, https://doi.org/10.3390/ma16093525.
[56] X. Yang, Q. Yang, J. Xu, C.-S. Lee, Bimetallic PtPd nanoparticles on Nafion–graphene film as catalyst for ethanol electro-oxidation, J. Mater. Chem. 22 (2012) 8057–8062, https://doi.org/10.1039/c2jm16916a.
[57] P. Heo, K. Ito, A. Tomita, T. Hibino, A proton-conducting fuel cell operating with hydrocarbon fuels, Angew. Chem. Int. Ed. 47 (2008) 7841–7844, https://doi.org/10.1002/anie.200801667.
[58] D.Y. Chung, K.-J. Lee, Y.-E. Sung, Methanol electro-oxidation on the Pt surface: revisiting the cyclic voltammetry interpretation, J. Phys. Chem. C 120 (2016) 9028–9035, https://doi.org/10.1021/acs.jpcc.5b12303.
[59] S. Stan, J. Woods, A. Daeschel, Investigation of the presence of OH radicals in electrolyzed NaCl solution by electron spin spectroscopy, J. Agric. Food Chem. 53 (2005) 4901–4905, https://doi.org/10.1021/jf047920b.
[60] N. Ohguri, A.Y. Nosaka, Y. Nosaka, Detection of OH radicals as the effect of Pt particles in the membrane of polymer electrolyte fuel cells, J. Power Sources 195 (2010) 4647–4652, https://doi.org/10.1016/j.jpowsour.2010.02.010.
[61] Y.Y. Ahn, S.Y. Yang, C. Choi, W. Choi, S. Kim, H. Park, Electrocatalytic activities of Sb-SnO_2 and Bi-TiO_2 anodes for water treatment: effects of electrocatalyst composition and electrolyte, Catal. Today 282 (2017) 57–64, https://doi.org/10.1016/j.cattod.2016.03.011.
[62] Y. Xue, Q. Luan, D. Yang, X. Yao, K. Zhou, Direct evidence for hydroxyl radical scavenging activity of cerium oxide nanoparticles, J. Phys. Chem. C 115 (2011) 4433–4438, https://doi.org/10.1021/jp109819u.
[63] C. Comninellis, Electrocatalysis in the electrochemical conversion/combustion of organic pollutants for waste water treatment, Electrochim. Acta 39 (1994) 1857–1862, https://doi.org/10.1016/0013-4686(94)85175-1.
[64] E. Peralta, G. Roa, J.A. Hemandez-Servin, Hydroxyl radicals quantification by UV spectrophotometry, Electrochim. Acta 129 (2014) 137–141, https://doi.org/10.1016/j.electacta.2014.02.047.
[65] Y. Liu, B. Sun, L. Wang, L.D. Wang, Characteristics of light emission and radicals formed by contact glow discharge electrolysis of an aqueous solution, Plasma Chem. Plasma Process. 32 (2012) 359–368, https://doi.org/10.1007/s11090-011-9347-7.
[66] K.W. Kim, Y.J. Kim, I.T. Kim, G.I. Park, E.H. Lee, Electrochemical conversion characteristics of ammonia to nitrogen, Water Res. 40 (2006) 1431–1441, https://doi.org/10.1016/j.watres.2006.01.042.
[67] K. Lundquist, P. Kristersson, Exhaustive laccase-catalysed oxidation of a lignin model compound (vanillyl glycol) produces methanol and polymeric quinoid products, Biochem. J. 229 (1985) 277–279, https://doi.org/10.1042/bj2290277.
[68] W.G. Trindade, W. Hoareau, I.A.T. Razera, R. Ruggiero, E. Frollini, A. Castellan, Phenolic thermoset matrix reinforced with sugar cane bagasse fibers: attempt to develop a new fiber surface chemical modification involving formation of quinones followed by reaction with furfuryl alcohol, Macromol. Mater. Eng. 289 (2004) (2004) 728–736, https://doi.org/10.1002/mame.200300320.
[69] H. Ma, T. Li, S. Wu, X. Zhang, Demethylation of a methoxy group to inhibit repolymerization during alkaline lignin pyrolysis, Fuel 286 (2021), 119394, https://doi.org/10.1016/j.fuel.2020.119394.
[70] Y.P. Wijaya, T. Grossmann-Neuhaeusler, R.D. Dhewangga Putra, K.J. Smith, C. S. Kim, E.L. Gyenge, Electrocatalytic hydrogenation of guaiacol in diverse electrolytes using a stirred slurry reactor, ChemSusChem 13 (2020) 629–639, https://doi.org/10.1002/cssc.201902611.
[71] Y.P. Wijaya, K.J. Smith, C.S. Kim, E.L. Gyenge, Synergistic effects between electrocatalyst and electrolyte in the electrocatalytic reduction of lignin model compounds in a stirred slurry reactor, J. Appl. Electrochem. 51 (2021) 51–63, https://doi.org/10.1007/s10800-020-01429-w.
[72] R.B. Lima, R. Raza, H. Qin, J. Li, M.E. Lindström, B. Zhu, Direct lignin fuel cell for power generation, RSC Adv. 3 (2013) 5083–5089, https://doi.org/10.1039/c3ra23418e.
[73] X. Zhao, J.Y. Zhu, Efficient conversion of lignin to electricity using a novel direct biomass fuel cell mediated by polyoxometalates at low temperatures, ChemSusChem 9 (2016) 197–207, https://doi.org/10.1002/cssc.201501446.
[74] D. Ouyang, D. Gao, Y. Qiang, X. Zhao, Highly-efficient conversion of lignin to electricity by nickel foam anode loaded with solid electrocatalysts, Appl. Catal. B Environ. 328 (2023), 122491, https://doi.org/10.1016/j.apcatb.2023.122491.